HHS Public Access

Author manuscript

ACS Appl Nano Mater. Author manuscript; available in PMC 2018 November 28.

Published in final edited form as:

ACS Appl Nano Mater. 2018 April 27; 1(4): 1741–1749. doi:10.1021/acsanm.8b00195.

Radiolabeled Angiogenesis-Targeting Croconaine Nanoparticles for Trimodality Imaging Guided Photothermal Therapy of Glioma

Longguang Tang[†,§,‡], **Xiaoli Sun**[‖,‡], **Nian Liu**[†], **Zijian Zhou**[§], **Fei Yu**[†], **Xianzhong Zhang**[†,*], **Xiaolian Sun**[⊥,*], and **Xiaoyuan Chen**[§,*]

[†]State Key Laboratory of Molecular Vaccinology and Molecular Diagnostics & Center for Molecular Imaging and Translational Medicine, School of Public Health, Xiamen University, Xiamen 361005, China

[⊥]Department of Pharmaceutical Analysis, China Pharmaceutical University, Nanjing 210009, China

[§]Laboratory of Molecular Imaging and Nanomedicine (LOMIN), National Institute of Biomedical Imaging and Bioengineering (NIBIB), National Institutes of Health, Bethesda, Maryland 20892, United States

[‖]School of Pharmaceutical Sciences, Wenzhou Medical University, Wenzhou 325035, China

Abstract

To meet the criteria of effective theranostics, biocompatible nanomedicine endowing intrinsic therapeutic and imaging properties have gained extraordinary momentum. In this study, an ultra-stable near-infrared (NIR) dye croconaine (CR780) was engineered with arginine-glycine-aspartic acid (RGD) peptide and polyethylene glycol (PEG), which was then self-assembled into uniform nanoparticles (NPs). These RGD-CR780-PEG5K assemblies were radiolabeled with ^{125}I through a facile standard Iodo-Gen method. The resulting [^{125}I]RGD-CR780-PEG5K NPs showed effective accumulation in $\alpha_v\beta_3$ integrin expressing glioblastoma, as evidenced by single photon emission computed tomography (SPECT)/CT and NIR fluorescence imaging. More importantly, high-resolution photoacoustic imaging revealed that these NPs selectively targeted to angiogenic tumor vessels. With the favorable tumor selective accumulation and high photothermal conversion efficiency, the [^{125}I]RGD-CR780-PEG5K NPs allowed thorough tumor ablation and inhibition of tumor relapse at a relatively low laser energy (0.5 W/cm^2). Overall, this work offers a proper methodology to fabricate tumor-targeted multi-modal nanotheranostic agents, providing great opportunity for precision imaging and cancer therapy.

Graphical abstract

[*]Corresponding Authors: zhangxzh@xmu.edu.cn, xiaolian86@gmail.com, shawn.chen@nih.gov.

[‡]**Author Contributions**

These authors equally contributed to this work

The authors declare no competing financial interest.

Supporting Information. The Supporting Information is available free of charge on the ACS Publications website. Materials, characterization of CRNPs, NIR laser-induced PTT effect, specificity of RGD-CR780-PEG5K for $\alpha_V\beta_3$ integrin, *in vitro* stability, cancer therapy, histological study and statistical analysis.

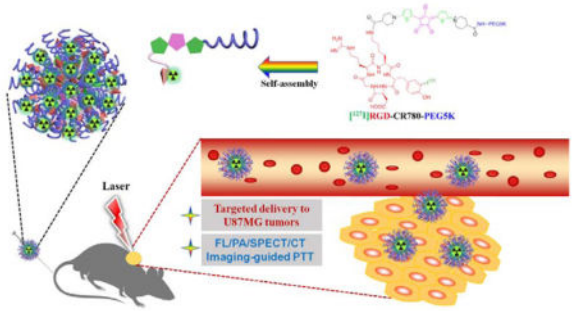

Keywords

croconaine nanoparticles; angiogenesis; SPECT/CT; photothermal therapy; glioma

1. INTRODUCTION

It is a key focus in nanomedicine to engineer compact materials with highly integrated modalities, which will exert widespread and far-reaching impact on molecular diagnostics, imaging and therapeutics.[1–3] Theranostic nanoparticles are attractive as they can concurrently deliver imaging probes and therapeutic agents to particular organs or tissues, allowing diagnosis and therapy of disease during the same process.[4–6] However, most of them struggle to enter into clinical trials, partially due to their structural complexity and potential toxicity to the normal tissues.[7] Therefore, although it is a great challenge, combining multiple components in one single biocompatible and effective molecule to create new multimodality theranostic agents has proven to be urgent and promising.[8]

Over the past decade, fluorescence imaging with near-infrared (NIR) dyes have become a very promising modality for monitoring various important biological behaviors *in vitro* and *in vivo*.[9] Croconaine dyes are a class of well-developed NIR dyes prepared by the condensation of croconic acid and a two-molar equivalent of a suitably reactive electron-donating aromatic or heterocyclic system.[10] Although they were less popular than squaraine dyes in imaging application,[11–14] the croconaine dyes have many advantages over the squaraine dyes, such as stronger absorption, greater photostability, absorption at longer wavelengths and better yield.[15–16] These extreme properties make croconaine dyes great candidates in bioimaging and photothermal therapy (PTT).[17–18] Recently, we reported the synthesis of CR780-PEG5K NPs with outstanding tumor theranostic capabilities.[19]

However, the tissue penetration depth of optical imaging is limited to millimeters, which may set a high bar for its clinical applications.[20] Moreover, to reduce the side effect on normal tissues under imaging guided PTT, a lower optical power density would be preferred. Radionuclide imaging such as single-photon emission computed tomography (SPECT) may represent an appropriate tool to obtain real-time and quantifiable information with high sensitivity and deep tissue penetration. Arg-Gly-Asp (RGD) is a well-known peptide with nanomolar affinity towards integrin $\alpha_v\beta_3$ which is overexpressed in many types of tumor cells and tumor vasculature.[21–23] Numerous studies have proved that RGD peptide modified nanoparticles can efficiently target tumors through both active and passive targeting.[24–26]

RGD can be directly radioiodinated with ^{123}I through standard Iodo-Gen method for SPECT imaging.[27,28] These highlights and findings inspired the current investigation of [^{125}I]RGD-CR780-PEG5K as a highly integrated multimodal theranostic agent, which combines the strengths of both small molecules and nanomaterials (Figure 1). In summary, compared with our previous report, there is a great improvement for the current study. Firstly, to realize its high sensitivity, deep tissue penetration and extraordinary spatial resolution, nuclear imaging (SPECT imaging) was integrated by radiolabeling the CRNPs. Secondly, to improve its cancer active targeting ability, RGD peptide was conjugated with the croconaine dye. Thirdly, to reduce the side effect on normal tissues but ensure the same photothermal therapeutic effect, a lower laser energy 0.5 W/cm^2 was applied in the PTT.

2. EXPERIMENTAL SECTION

Synthesis of compound 3 (Tyr-CR780-PEG5K) and 6 (RGD-CR780-PEG5K)

Compound **1** (**CR780-PEG5K**) was first prepared as we previously described.[19] Then compound **1** (0.1 mmol), HOBt (0.2 mmol) and EDC·HCl (0.2 mmol) were dissolved in 20 mL DMF with 0.2 mmol DIPEA. The methyl 2-amino-3-(4-hydroxyphenyl)propanoate (**2**) (0.1 mmol) was then added to the above solution at 0 °C and kept stirring for 30 min. After additional reaction for 24 h at room temperature, the solvent was evaporated to yield a black crude product. Then, water (2 ml) was gradually added and stirred for another 2 h. Then, the sample was purified by dialysis in deionized water.. The final product **3** was obtained by freeze-drying (yield 63%). MALDI-TOF spectrum of **3**, expected MW ~5495, measured MW about ~5496.

The compound **6** (**RGD-CR780-PEG5K)** was synthesized in a similar way, using cyclo(RGDyK) instead of **2**. MALDI-TOF spectrum of **6**, expected MW ~5919, measured MW about ~5920.

Preparation of Croconaine Nanoparticles

They were prepared as reported previously[29]. Briefly, Tyr-CR780-PEG5K or RGD-CR780-PEG5K (2 μmol) was dissolved in chloroform (200 μl), then dried to yield a film layer. For formulation of nanoparticles, the film layer was rehydrated with 500 μl of phosphate buffered saline (PBS) and the suspension was sonicated for 10 min, yielding uniform sized croconaine nanoparticles. Morphology of the nanoparticles was characterized by TEM and DLS. The diluted solution of croconaine nanoparticles was used for further *in vitro* and *in vivo* studies.

Radioiodination of 4 ([^{125}I]Tyr-CR780-PEG5K) and 7 ([^{125}I]RGD-CR780-PEG5K)

3 or **6** was iodinated using the Iodo-Gen method.[27] Iodo-Gen was dissolved in methylene chloride and coated onto glass tubes by evaporation. These tubes were stored covered and refrigerated until use. **3** or **6** (25–50 nmol) was added to the Iodo-Gen tube followed by 1–2 mCi ^{125}I as NaI in CH_3CN. The solution was vibrated at 25 °C for another 5 min. Iodination process was stopped by adding $Na_2S_2O_5$. Then it was filtered and purified by a semipreparative radio-HPLC column (Luna C-18, 5 μm, 10×250 mm; Thermo).

Stability of Radioactive Products *in Vitro*

[^{125}I]Tyr-CR780-PEG5K and [^{125}I]RGD-CR780-PEG5K (370 KBq) after HPLC purification were dissolved in 100 μl of normal saline, and then mixed with 500 μL of normal saline or mouse serum at 37 °C, respectively. The detached radioidione was tested by radio-HPLC.

In vivo imaging

The animal experiments were performed following a protocol approved by the Animal Care and Use Committee (CC/ACUCC) of Xiamen University. U87MG tumor-bearing nude mice were obtained by subcutaneously injecting a suspension of 4×10^6 U87MG cells. When the tumor size was about 100 mm^3, 100 μL of Tyr-CR780-PEG5K, RGD-CR780-PEG5K or RGD-CR780-PEG5K + c(RGDyK) (block) (1 mM, n = 4/group) was intravenously injected respectively for fluorescence imaging by Carestream FX Pro at 1, 6 and 24 h, and PA imaging on Endra Nexus128 (Ann Arbor, MI) at 6 h. A small-animal SPECT/CT imaging study was also conducted on U87MG tumor-bearing mice by intravenous injection with 18.5 MBq of [^{125}I]Tyr-CR780-PEG5K or [^{125}I]RGD-CR780-PEG5K. The blocking study was also performed in U87MG mice (n = 4 per group) by co-injection of 18.5 MBq of [^{125}I]RGD-CR780-PEG5K with an excess dose of the c(RGDyK) (200 μg). The SPECT images were obtained using a nanoScan-SPECT/CT preclinical scanner with 35 keV for ^{125}I. All images were acquired in the same manner, reconstructed and analyzed with Nucline software (Mediso Medical Imaging System).

Biodistribution

The distribution of [^{125}I]Tyr-CR780-PEG5K and [^{125}I]RGD-CR780-PEG5K in tumors and major organs (n = 4/group) were evaluated on female nude mice bearing U87MG tumor xenografts by injection of 0.18 MBq [^{125}I]Tyr-CR780-PEG5K, [^{125}I]RGD-CR780-PEG5K or RGD-CR780-PEG5K + c(RGDyK) (block, 200 μg). The mice were sacrificed and dissected at 6 h post-injection. Samples of tumor, blood, liver (without gallbladder) and other major organs were collected and weighted. The radioactivity was measured with a γ-counter. The data were shown as mean ± SD percentage injected dose per gram (%ID/g).

Blood Half-Life

U87MG tumor-bearing mice with tumor size around 200 mm^3 were injected with [^{125}I]RGD-CR780-PEG5K (150 μL, 100 μCi). After collecting the blood samples from the tail vein at different time points, the radioactivity was detected by a well-type scintillation detector. Blood half-life of [^{125}I]RGD-CR780-PEG5K was analyzed with the Drug and Statistics for windows 2.0 software.[30]

In Vitro Hemolysis Assay

The *in vitro* hemolysis assay was conducted following a previously reported method.[31]

2. RESULTS AND DISCUSSION

Synthesis and Characterization of Croconaine Nanoparticles

The detailed synthetic routes of [^{125}I]Tyr-CR780-PEG5K and [^{125}I]RGD-CR780-PEG5K are shown in Scheme 1. CR780-PEG5K was first synthesized according to our previously reported method.[19] The tyrosine and RGD were covalently linked to this compound *via* an amidation reaction. Tyr-CR780-PEG5K and RGD-CR780-PEG5K were confirmed by ^{1}H NMR (Figure S1) and MALDI-TOF MS (Figure S2 C–D). Similar to what we have previously observed, these two amphiphilic compounds could also self-assemble into nanostructures because of interactions among individual hydrophobic croconaine molecules. DLS and TEM measurements revealed that Tyr-CR780-PEG5K and RGD-CR780-PEG5K formed nanoscale particles with sizes around 66 ± 2 nm and 40 ± 3 nm, respectively (Figure S3 A–D), at concentrations greater than 10 nM, and that the nanoparticle sizes were almost unchanged within one day incubation in serum, which were 56 ± 2 nm and 38 ± 2 nm, respectively (Figure S3 E–F). [^{125}I]Tyr-CR780-PEG5K and [^{125}I]RGD-CR780-PEG5K were both prepared using the standard Iodo-Gen method in high radiochemical yield of 89.2 ± 4.5% (n = 6) and the radiochemical purity was more than 95% (Figure S2 A–B). The purified [^{125}I]Tyr-CR780-PEG5K and [^{125}I]RGD-CR780-PEG5K were stable in mouse serum, and free iodide was undetectable after incubation at 37 °C for 24 h (Figure S4). The stability of the croconaine nanoparticles was also examined under physiological conditions. Tyr-CR780-PEG5K NPs and RGD-CR780-PEG5K NPs were incubated in DMEM (with 10% FBS) and PBS for 24 h. No obvious aggregation was observed, indicating the excellent stability of croconaine nanoparticles (Figure S5).

PA, Optical, Photothermal Properties and Photothermal Stability of the Croconaine Nanoparticles

In our previous report, CR780-PEG5K NPs showed favorable optical properties, excellent photothermal conversion efficiency as well as ideal chemical and thermal stability. In this study, the tyrosine and RGD peptide was conjugated with CR780-PEG5K to form Tyr-CR780-PEG5K and RGD-CR780-PEG5K, respectively. As expected, compared to the CR780-PEG5K NPs at the same concentration (30 μM), the modified croconaine nanoparticles exhibited no significant change of its physicochemical properties (Figure 2A–H). To determine whether heating could compromise its chemical structure and optical properties, the infrared absorbance and fluorescence spectra were acquired before and after laser irradiation (0.5 W/cm^2, 20 min) with 30 μM samples. No obvious change in optical properties was observed (Figure 2D–F) even though the temperature reached almost 65 °C (Figure 2A–B). Thus, we believe that Tyr-CR780-PEG5K NPs and RGD-CR780-PEG5K NPs maintained similar optical properties of CR780-PEG5K NPs.

In Vitro Specificity and PTT Efficacy of the Agents

To estimate the active targeting ability of the nanoparticles for $\alpha_v\beta_3$ integrin, U87MG cells (integrin $\alpha_v\beta_3$ positive)[32] were treated with Tyr-CR780-PEG5K NPs, RGD-CR780-PEG5K NPs, or RGD-CR780-PEG5K NPs plus free RGD peptide (30 μM CR780 equivalent) for 4 h. As shown in Figure 3A, the group treated with RGD-CR780-PEG5K NPs demonstrated much stronger fluorescence signal than that treated with Tyr-CR780-PEG5K NPs. The

competitive binding assay was also performed to study the specificity of RGD-CR780-PEG5K NPs towards U87MG cells. The $\alpha_v\beta_3$ integrin receptors on U87MG cells were initially saturated by excess amount of free RGD peptide and then added RGD-CR780-PEG5K NPs. After 4 h incubation, fluorescence signal was much weaker than that without $\alpha_v\beta_3$ integrin blocking. Similarly, the cell uptake experiment was also done by incubating the ^{125}I-labeled croconaine nanoparticles for different time courses. It was obvious that the cells adding [^{125}I]RGD-CR780-PEG5K reached the highest radioactivity at 4 h, which was significantly higher than that in [^{125}I]Tyr-CR780-PEG5K group and blocking group (Figure 3B). These results suggested that RGD-CR780-PEG5K NPs and [^{125}I]RGD-CR780-PEG5K are $\alpha_v\beta_3$ integrin specific and consequently are able to reach the tumor site by integrin-mediated targeting. After the cells were treated with RGD-CR780-PEG5K NPs and Tyr-CR780-PEG5K NPs (30 μM) for 4 h, they were exposed to laser irradiation (808 nm, 0.5 W/cm^2, 10 min). The calcein AM and propidium iodide (PI) staining as well as MTT were done to calculate the cell viabilities. The cell viabilities of Tyr-CR780-PEG5K NPs group, RGD-CR780-PEG5K NPs group and block group after 10 min irradiation were 53.2 ± 3.2, 12.4 ± 2.1 and 91.32 ± 2.5%, respectively (Figure 3D). However, all the non-irradiated groups revealed almost no dead cells, indicating their good biocompatibility without obvious cytotoxicity. Accordingly, RGD-CR780-PEG5K NPs can specifically target the U87MG cells and facilitate cell uptake.

In Vivo Fluorescence and Photoacoustic Imaging of the Croconaine Nanoparticles

Encouraged by the *in vitro* results, the NIR fluorescence imaging of these samples were monitored *in vivo*. U87MG tumor mice were intravenously injected with RGD-CR780-PEG5K NPs and Tyr-CR780-PEG5K NPs (100 μL, 1 mM), and fluorescence images were acquired at different time points. As illustrated in Figure 4A, the NPs revealed a time-dependent biodistribution profile in the mice. Although the NPs were widely dispersed among the whole body within 1 h postinjection, at later time points (e.g., after 6 h and later), RGD-CR780-PEG5K NPs showed obviously higher tumor accumulation as compared with Tyr-CR780-PEG5K NPs without RGD. Furthermore, to verify the receptor specificity, blocking experiments were also done by injecting free c(RGDyK) peptide 30 min before the administration of RGD-CR780-PEG5K NPs, the tumor uptakes of RGD-CR780-PEG5K NPs at 6 h and 24 h postinjection were significantly inhibited by the preinjection of c(RGDyK) peptide (Figure 4A–B).

Since the croconaine nanoparticles had a strong light absorbance in the NIR region, PA imaging was employed to witness the blood vessel distribution of CRNPs in the tumor area. As displayed in Figure **4C–D**, the tumor PA contrast of RGD-CR780-PEG5K NPs group at 6 h postinjection was considerably higher than that of the other two groups and before injection, which was consistent with the fluorescence imaging results. These outcomes demonstrated that the tumor specific accumulation of RGD-CR780-PEG5K NPs was mediated by the RGD peptide.

SPECT/CT Imaging

The limited tissue-penetration property of optical imaging may prevent its clinical application, radionuclide imaging represents an appropriate tool to obtain real-time and

quantifiable information about receptor expression with high sensitivity and spatial resolution. Therefore, SPECT/CT imaging was performed to investigate its specific targeting and to optimize the time point for photothermal therapy by examining mice administered with [^{125}I]RGD-CR780-PEG5K, [^{125}I]Tyr-CR780-PEG5K, or [^{125}I]RGD-CR780-PEG5K plus free RGD peptide (18.5 MBq/mouse). SPECT/CT imaging illustrated that the radioactive signal in the tumor area of [^{125}I]RGD-CR780-PEG5K was definitely stronger than that of [^{125}I]Tyr-CR780-PEG5K at 6 h post-injection (Figure 5A). Nevertheless, in the blocking group, the radioactive signal was significantly decreased, and the tumor accumulation of [^{125}I]RGD-CR780-PEG5K was marginal.

Biodistribution

The mice were sacrificed after SPECT/CT imaging, and the biodistribution of radiolabeled nanoparticles in major organs were recorded as the percentage of injected dose per gram tissue (%ID/g) (Figure 5B). Unlike most of the other nanomaterials which mainly accumulated in the liver,[33–34] both [^{125}I]RGD-CR780-PEG5K and [^{125}I]Tyr-CR780-PEG5K had predominant renal clearance. Tumor uptake of [^{125}I]RGD-CR780-PEG5K was also significantly reduced in the presence of free RGD peptide. The tumor uptake of [^{125}I]Tyr-CR780-PEG5K was 2.74 ± 0.47 %ID/g at 6 h, which was notably less than that of [^{125}I]RGD-CR780-PEG5K ($p < 0.05$). These results confirmed the SPECT/CT findings. Most of the nanoparticles have the disadvantages of high accumulation and retention in the reticuloendothelial system (RES), which may bring potential long-term toxicity and hamper their clinical translation.[35] To minimize nonspecific uptake by the RES, the croconaine nanoparticles in this study were prepared with renal clearance, which allows the nanoparticles to be effectively cleared through the kidneys.

The pharmacokinetic properties of [^{125}I]RGD-CR780-PEG5K was also assessed, which showed that the blood level of the tracer declined over time and had only about 2 %ID/g remaining at 6 h after injection (Figure 5C). The blood clearance half-life ($t_{1/2}$) was calculated to be 2.21 ± 0.12 h by applying non-compartmental analysis of Drug and Statistics for windows 2.0 software.[30]

In vivo PTT

The *in vivo* PTT effect of the probes was evaluated by tail vein injection with PBS or different probes (100 μL, 2 mM). U87MG tumor mice were randomly divided into seven groups (n= 5/group): PBS, PBS + laser, Tyr-CR780-PEG5K, Tyr-CR780-PEG5K + laser, RGD-CR780-PEG5K, RGD-CR780-PEG5K + laser, RGD-CR780-PEG5K + free c(RGDyK) + laser. In our previous report, the tumor can be eliminated by CR780-PEG5K NPs with 808 nm NIR irradiation (1 W/cm^2, 10 min). However, the excessively high optical power density (1 W/cm^2) and the relatively low specific uptake in tumor may lead to the injury of normal tissues around the tumor tissues. Therefore, to avoid the side effect to normal tissues, we conducted the PPT at a much lower laser power density of 0.5 W/cm^2. The laser irradiation (0.5 W/cm^2, 10 min) was conducted at 6 h post-injection when tumor uptake peaked according to the *in vivo* imaging, followed by size determination with a caliper every other day. The temperature change *in vivo* was monitored by an IR thermal camera, which illustrated that the tumor temperature rose to 50 °C at 6 min after laser

irradiation for the RGD-CR780-PEG5K + laser group, while after blocking with free RGD, only reached 35 °C. Without receptor mediated targeting, however, it reached only 45 °C for the Tyr-CR780-PEG5K + laser group (Figure 6A–B). The dark-red skin at the tumor site was found in both RGD-CR780-PEG5K and Tyr-CR780-PEG5K + laser groups after laser treatment, indicating that tissue burns were caused by the local photothermal effect, while no remarkable change was observed in the blocking group (Figure 6E). Tumors from RGD-CR780-PEG5K + laser group entirely disappeared on day 14 without regrowth in the next 40 days, while it reappeared in the Tyr-CR780-PEG5K + laser group with delayed growth. In marked contrast, tumors in the other control groups, including PBS injection without or with laser irradiation, as well as croconaine nanoparticles injection without laser exposure, all showed rapid growth (Figure 6C). Remarkably, mice after PTT treatment with RGD-CR780-PEG5K were tumor-free and survived for more than 40 days, while in the other six control groups the average life spans of mice were less than 24 days, clearly suggesting that RGD-CR780-PEG5K was effective for *in vivo* photothermal ablation of tumors (Figure 6D). Particularly, as our tracer can precisely target tumor angiogenic vessels that play an important role for tumor growth, destruction to tumor microvasculature may hence be a valuable mechanism for cancer inhibition. Furthermore, through the same method used for ^{125}I labeling, RGD-CR780-PEG5K can be labeled with ^{131}I, a beta- and gamma-ray emitter broadly used for cancer radiotherapy in the clinic, to allow simultaneous PTT and radiotherapy, which will likely yield synergistic anticancer effect by employing a single nanoscale theranostic agent.

Finally, we studied the potential toxic effect of RGD-CR780-PEG5K NPs in normal mice with 2-fold of the therapy dose, which showed negligible organ damage or abnormalities according to the H&E staining of main organs from mice 7 days post-treatment (Figure S6). These results illustrated that RGD-CR780-PEG5K NPs had no noticeable short-term toxicity in mice in the present study. Furthermore, to investigate the biocompatibility of RGD-CR780-PEG5K NPs, hemolysis assay was conducted to explore the interaction between CRNPs and blood components (Figure S7), and no hemolysis of RBCs was observed in the presence of the highest experimental concentration, manifesting their favorable blood compatibility and biocompatibility.

4. CONCLUSION

In summary, a novel class of radiolabeled integrin targeted nanotheranostic agent comprised of croconaine nanoparticles (CRNPs) has been developed. The resulting CRNPs showed highly integrated properties of the all-in-one molecule, including nuclear, optical, acoustic and thermal responses, which allow SPECT/CT imaging, optical imaging, PA imaging and photothermal therapy. We envision that the CRNPs will also be able to load anticancer drugs and be radiolabeled with radionuclide ^{131}I for chemo- and radio-thermal combined therapy.

Supplementary Material

Refer to Web version on PubMed Central for supplementary material.

Acknowledgments

This research was supported in part by the Intramural Research Program, National Institute of Biomedical Imaging and Bioengineering (NIBIB), National Institutes of Health (NIH), National Key Research and Development Program of China (No. 2016YFA0203600), National Natural Science Foundation of China (Nos. 81571743, 51502251), Fundamental Research Funds for Xiamen University (No. 20720160067) and Natural Science Foundation of Fujian Province (Nos. 2014Y2004).

References

1. Jin YD, Jia CX, Huang SW, O'Donnell M, Gao XH. Multifunctional Nanoparticles as Coupled Contrast Agents. Nat Commun. 2010; 1(4):41–48. [PubMed: 20975706]
2. Kamkaew A, Cheng L, Goel S, Valdovinos HF, Barnhart TE, Liu Z, Cai W. Cerenkov Radiation Induced Photodynamic Therapy Using Chlorin e6-Loaded Hollow Mesoporous Silica Nanoparticles. Acs Appl Mater Interfaces. 2016; 8(40):26630–26637. [PubMed: 27657487]
3. Min Y, Caster JM, Eblan MJ, Wang AZ. Clinical Translation of Nanomedicine. Chem Rev. 2015; 115(19):11147–11190. [PubMed: 26088284]
4. Lee DE, Koo H, Sun IC, Ryu JH, Kim K, Kwon IC. Multifunctional Nanoparticles for Nultimodal Imaging and Theragnosis. Chem Soc Rev. 2012; 41(7):2656–2672. [PubMed: 22189429]
5. Zhao J, Yang Y, Han X, Liang C, Liu J, Song X, Ge Z, Liu Z. Redox-Sensitive Nanoscale Coordination Polymers for Drug Delivery and Cancer Theranostics. Acs Appl Mater Interfaces. 2017; 9(28):23555–23563. [PubMed: 28636308]
6. Lim EK, Kim T, Paik S, Haam S, Huh YM, Lee K. Nanomaterials for Theranostics: Recent Advances and Future Challenges. Chem Rev. 2015; 115(1):327–394. [PubMed: 25423180]
7. Kagan VE, Bayir H, Shvedova AA. Nanomedicine and Nanotoxicology: Two Sides of the Same Coin. Nanomedicine. 2005; 1(4):313–316. [PubMed: 17292104]
8. Chen G, Roy I, Yang C, Prasad PN. Nanochemistry and Nanomedicine for Nanoparticle-based Diagnostics and Therapy. Chem Rev. 2016; 116(5):2826–2885. [PubMed: 26799741]
9. van Dam GM, Themelis G, Crane LM, Harlaar NJ, Pleijhuis RG, Kelder W, Sarantopoulos A, de Jong JS, Arts HJ, Ag VDZ. Intraoperative Tumor-Specific Fluorescence Imaging in Ovarian Cancer by Folate Receptor-α, Targeting: First in-human Results. Nat Med. 2011; 17(10):1315–1319. [PubMed: 21926976]
10. Sovera VDL, Suescun L, Bellomo A, Gonzalez D. Chemoenzymatic Synthesis of Triazololactams Structurally Related to Pancratistatin. Eur J Org Chem. 2017; 2017(27):3912–3916.
11. Seitz G, Imming P. Oxocarbons and Pseudooxocarbons. Chem Rev. 1992; 92(6):1227–1260.
12. Ajayaghosh A. Chemistry of Squaraine-derived Materials: Near-IR Dyes, Low Band Gap Systems, and Cation Sensors. Acc Chem Res. 2005; 38(6):449–459. [PubMed: 15966711]
13. Beverina L, Salice P. Squaraine Compounds: Tailored Design and Synthesis towards a Variety of Material Science Applications. Eur J Org Chem. 2010; 2010(7):1207–1225.
14. Sreejith S, Joseph J, Lin M, Menon NV, Borah P, Ng HJ, Loong YX, Kang Y, Yu SW, Zhao Y. Near-Infrared Squaraine Dye Encapsulated Micelles for in Vivo Fluorescence and Photoacoustic Bimodal Imaging. ACS Nano. 2015; 9(6):5695–5704. [PubMed: 26022724]
15. Yasui S, Matsuoka M, Kitao T. Syntheses and Some Properties of Infrared-absorbing Croconium and Related Dyes. Dyes Pigm. 1989; 10(1):13–22.
16. Liu L, Liu MH, Deng LL, Lin BP, Yang H. Near-Infrared Chromophore Functionalized Soft Actuator with Ultrafast Photoresponsive Speed and Superior Mechanical Property. J Am Chem Soc. 2017; 139(33):11333–11336. [PubMed: 28786668]
17. Guha S, Shaw GK, Mitcham TM, Bouchard RR, Smith BD. Croconaine Rotaxane for Acid Activated Photothermal Heating and Ratiometric Photoacoustic Imaging of Acidic pH. Chem Commun. 2016; 52(1):120–123.
18. Spence GT, Hartland GV, Smith BD. Activated Photothermal Heating Using Croconaine Dyes. Chem Sci. 2013; 4(11):4240–4244.

19. Tang L, Zhang F, Yu F, Sun W, Song M, Chen X, Zhang X, Sun X. Croconaine Nanoparticles with Enhanced Tumor Accumulation for Multimodality Cancer Theranostics. Biomaterials. 2017; 129:28–36. [PubMed: 28324863]
20. Weissleder R. Scaling Down Imaging: Molecular Mapping of Cancer in Mice. Nat Rev Cancer. 2002; 2(1):11–18. [PubMed: 11902581]
21. Cai W, Chen X. Multimodality Molecular Imaging of Tumor Angiogenesis. J Nucl Med. 2008; 49(Suppl 2):113s–128s. [PubMed: 18523069]
22. Ye Y, Chen X. Integrin Targeting for Tumor Optical Imaging. Theranostics. 2011; 1(1):102–126. [PubMed: 21546996]
23. Chen K, Chen X. Integrin Targeted Delivery of Chemotherapeutics. Theranostics. 2011; 1(1):189–200. [PubMed: 21547159]
24. Lin X, Xie J, Niu G, Zhang F, Gao H, Yang M, Quan Q, Aronova MA, Zhang G, Lee S, Leapman R, Chen X. Chimeric Ferritin Nanocages for Multiple Function Loading and Multimodal Imaging. Nano Lett. 2011; 11(2):814–819. [PubMed: 21210706]
25. Millard M, Odde S, Neamati N. Integrin targeted therapeutics. Theranostics. 2011; 1:154–188. [PubMed: 21547158]
26. Zhen Z, Tang W, Chen H, Lin X, Todd T, Wang G, Cowger T, Chen X, Xie J. RGD Modified Apoferritin Nanoparticles for Efficient Drug Delivery to Tumors. ACS Nano. 2013; 7(6):4830–4837. [PubMed: 23718215]
27. NatCommunAli SA, Warren SD, Richter KY, Badger CC, Eary JF, Press OW, Krohn KA, Bernstein ID, Nelp WB. Improving the Tumor Retention of Radioiodinated Antibody: Aryl Carbohydrate Adducts. Cancer Res. 1990; 50(3 Suppl):783s–788s. [PubMed: 2297724]
28. Zmuda F, Malviya G, Blair A, Boyd M, Chalmers AJ, Sutherland A, Pimlott SL. Synthesis and Evaluation of a Radioiodinated Tracer with Specificity for Poly(ADP-ribose) Polymerase-1 (PARP-1) in Vivo. J Med Chem. 2015; 58(21):8683–8693. [PubMed: 26469301]
29. Lee Y, Kim H, Kang S, Lee J, Park J, Jon S. Bilirubin Nanoparticles as a Nanomedicine for Anti-inflammation Therapy. Angew Chem Int Ed Engl. 2016; 55(26):7460–7463. [PubMed: 27144463]
30. Wang Q, Yang S, Jiang C, Li J, Wang C, Chen L, Jin Q, Song S, Feng Y, Ni Y. Discovery of Radioiodinated Monomeric Anthraquinones as a Novel Class of Necrosis Avid Agents for Early Imaging of Necrotic Myocardium. Sci Rep. 2016; 6:21341–21349. [PubMed: 26878909]
31. Dong K, Liu Z, Li Z, Ren J, Qu X. Hydrophobic Anticancer Drug Delivery by a 980 nm Laser Driven Photothermal Vehicle for Efficient Synergistic Therapy of Cancer Cells In Vivo. Adv Mater. 2013; 25:4452–4458. [PubMed: 23798450]
32. Cai W, Shin DW, Chen K, Gheysens O, Cao Q, Wang SX, Gambhir SS, Chen X. Peptide-labeled Near-infrared Quantum Dots for Imaging Tumor Vasculature in Living Subjects. Nano Lett. 2006; 6(4):669–676. [PubMed: 16608262]
33. Longmire M, Choyke PL, Kobayashi H. Clearance Properties of Nano-sized Particles and Molecules as Imaging Agents: Considerations and Caveats. Nanomedicine. 2008; 3(5):703–717. [PubMed: 18817471]
34. Choi HS, Liu W, Misra P, Tanaka E, Zimmer JP, Ipe BI, Bawendi MG, Frangioni JV. Renal Clearance of Quantum Dots. Nat Biotechnol. 2007; 25(10):1165–1170. [PubMed: 17891134]
35. Yang RS, Chang LW, Wu JP, Tsai MH, Wang HJ, Kuo YC, Yeh TK, Yang CS, Lin P. Persistent Tissue Kinetics and Redistribution of Nanoparticles, Quantum Dot 705, in Mice: ICP-MS Quantitative Assessment. Environ Health Persp. 2007; 115(9):1339–1343.

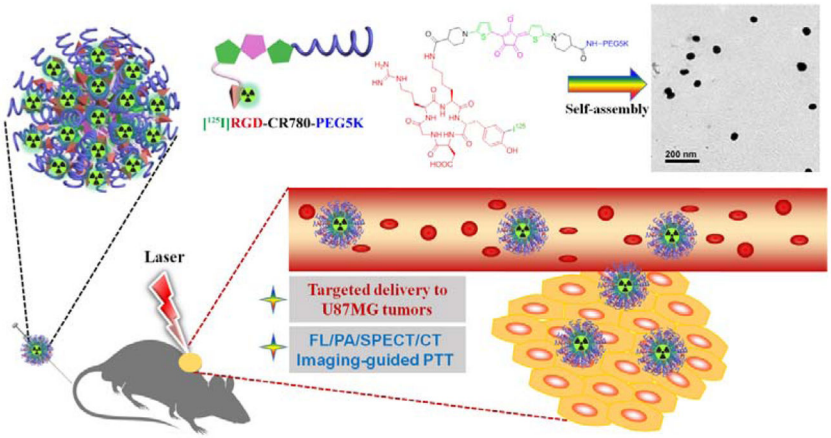

Figure 1.

Schematic illustration of radiolabled angiogenesis-targeting croconaine nanoparticles ([^{125}I]RGD-CR780-PEG5K NPs) for tumor $\alpha_v\beta_3$ integrin multimodality imaging guided photothermal therapy.

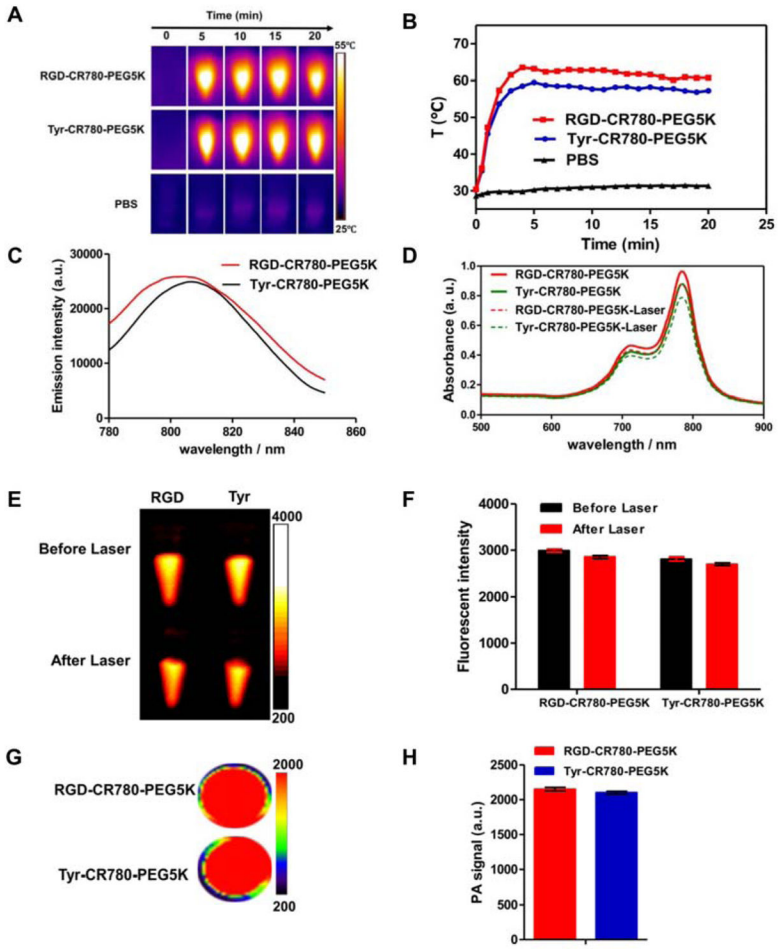

Figure 2.

(A) Real-time thermal imaging and (B) temperature changes of RGD-CR780-PEG5K, Tyr-CR780-PEG5K in aqueous solutions (30 μM) and PBS with laser irradiation (808 nm, 0.5 W/cm^2 for 20 min). (C) Emission spectra of RGD-CR780-PEG5K and Tyr-CR780-PEG5K in aqueous solutions (30 μM) excited at 760 nm. (D–F) Vis-NIR spectra (D), Fluorescent images (E) and quantification of corresponding intensities of RGD-CR780-PEG5K and Tyr-CR780-PEG5K at 30 μM before and after laser irradiation (808 nm, 0.5 W/cm^2 for 20 min). (G–H) PA images (G) and corresponding amplitude (H) of RGD-CR780-PEG5K and Tyr-CR780-PEG5K at 30 μM. The data are shown as mean ± SD (n = 3).

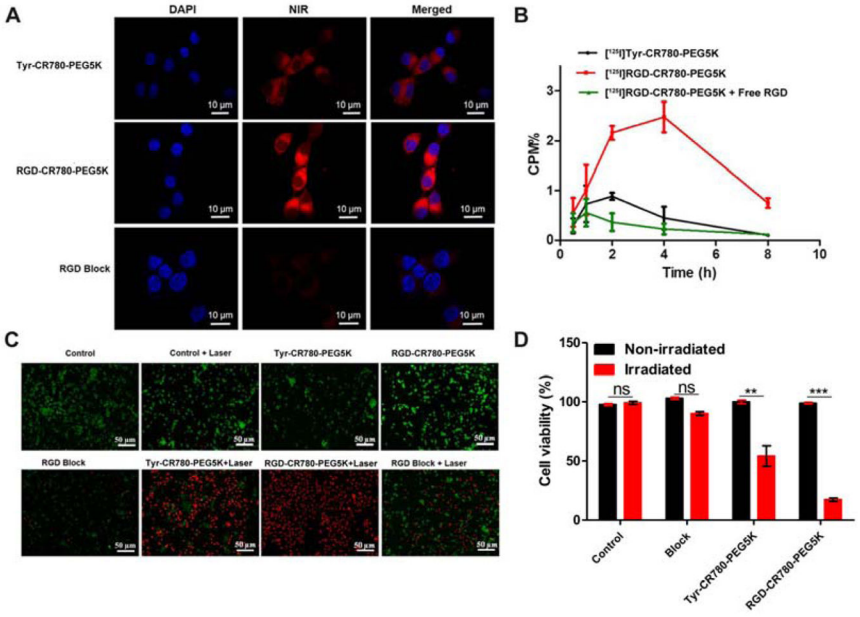

Figure 3.

(A) Subcellular localization of Tyr-CR780-PEG5K, RGD-CR780-PEG5K and RGD-CR780-PEG5K + free c(RGDyK) (block) (30 μM). Co-localization of the NIR dyes (Ex = 633 nm) with DAPI at 4 h in U87MG cells as imaged by confocal microscope. (B) Uptake of [^{125}I]Tyr-CR780-PEG5K, [^{125}I]RGD-CR780-PEG5K and [^{125}I]RGD-CR780-PEG5K + free c(RGDyK) (block) (37 KBq) by U87MG cells at different times. (C–D) Fluorescence images of calcein AM/PI co-stained U87MG cells (C) and Cell viability determined by MTT assay (D) after incubation with Tyr-CR780-PEG5K, RGD-CR780-PEG5K and RGD-CR780-PEG5K + free c(RGDyK) (block) (30 μM) for 4 h with or wihtout being exposed to 808 nm laser at 0.5 W/cm^2 for 5 min. The data are shown as mean ± SD (n = 3), ** $P < 0.01$, *** $P < 0.001$, compared with non-irradiated group.

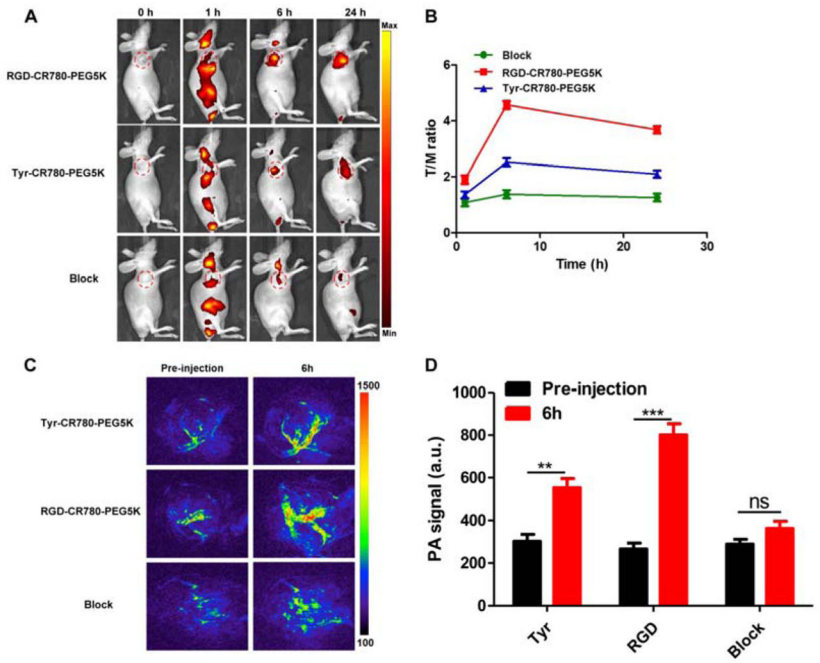

Figure 4.

(A–B) Whole-body NIR fluorescent imaging (A) and correspondingly tumor-to-muscle ratios (B) of U87MGtumor-bearing mice after intravenous (i.v.) injection of Tyr-CR780-PEG5K, RGD-CR780-PEG5K and RGD-CR780-PEG5K + free c(RGDyK) (block). Images were acquired at indicated time points and the color bar indicates radiant efficiency (low, 2.5×10^6; high, 4.80×10^6). Red circles were used to indicate tumors. (C–D) PA imaging (C) and PA intensities (D) of tumor tissues in U87MG tumor-bearing mice at 6 h after injection. $n = 4$ per group, ** $P < 0.01$, *** $P < 0.001$.

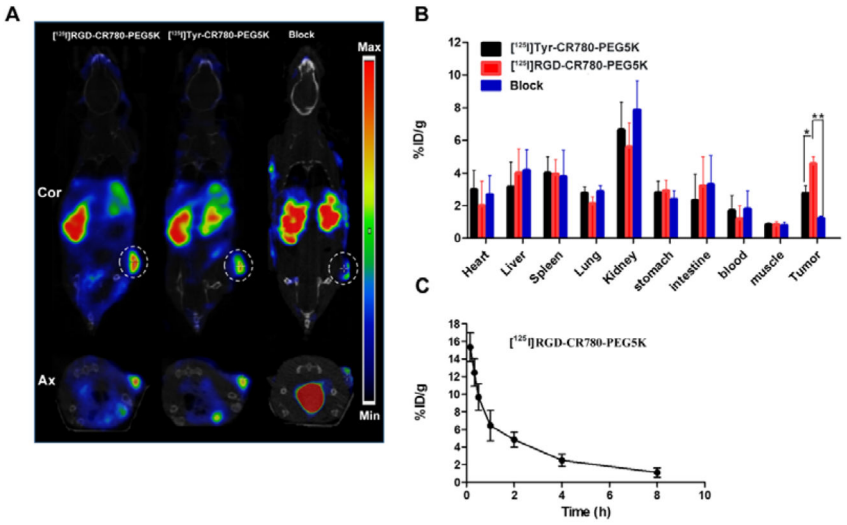

Figure 5.

In vivo behavior of the probes. (A) SPECT/CT imaging of tumor-bearing mice 6 h after intravenous injection with [^{125}I]Tyr-CR780-PEG5K, [^{125}I]RGD-CR780-PEG5K, or [^{125}I]RGD-CR780-PEG5K probes plus free RGD peptide (100 μL, 0.15 mM), at a radiation dose of 18.5 MBq. (B) Biodistributions of the probes 6 h after injection. (C) Blood clearance profile of [^{125}I]RGD-CR780-PEG5K after intravenous injection. The data are shown as mean ± SD (n = 4), * $P < 0.05$, ** $P < 0.01$.

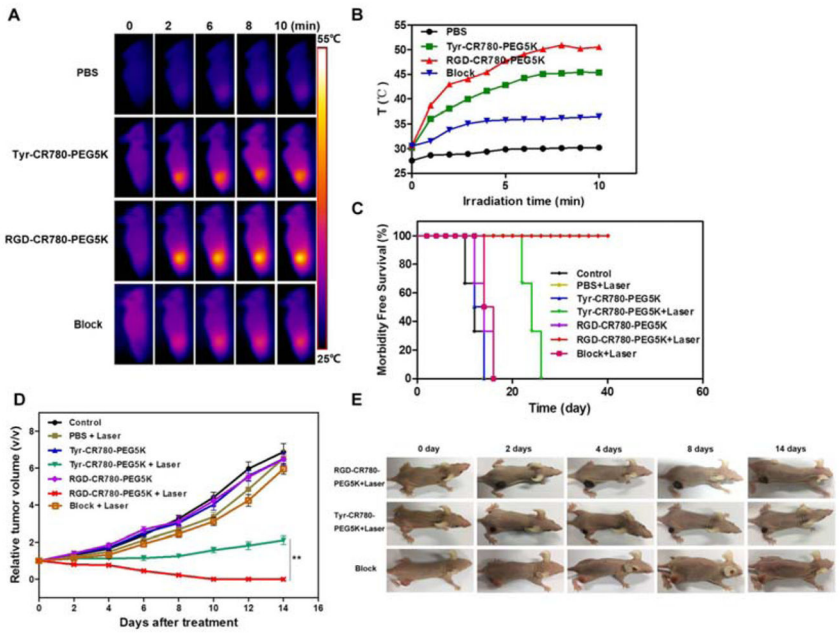

Figure 6.

In vivo PTT effect. (A) Thermal images of U87MG tumor-bearing mice i.v. treated with 100 μL PBS, Tyr-CR780-PEG5K, RGD-CR780-PEG5K or RGD-CR780-PEG5K + c(RGDyK) (block, 200 μg) (2 mM) and illuminated with 808 nm laser (0.5 W/cm^2, 10 min) at 6 h post-injection. (B) Quantitative analysis of temperature changes in tumor area. (C) U87MG tumor growth rate in each groups after indicated treatments. Tumor volumes were normalized to their initial size (n = 5 per group). (D) Survival curves of tumor-bearing mice after various treatments. RGD-CR780-PEG5K + laser group showed 100% survival over 40 days. (E) Representative images of mice bearing U87MG tumors after treatments. The data are shown as mean ± SD (n = 3), ** $P < 0.01$.

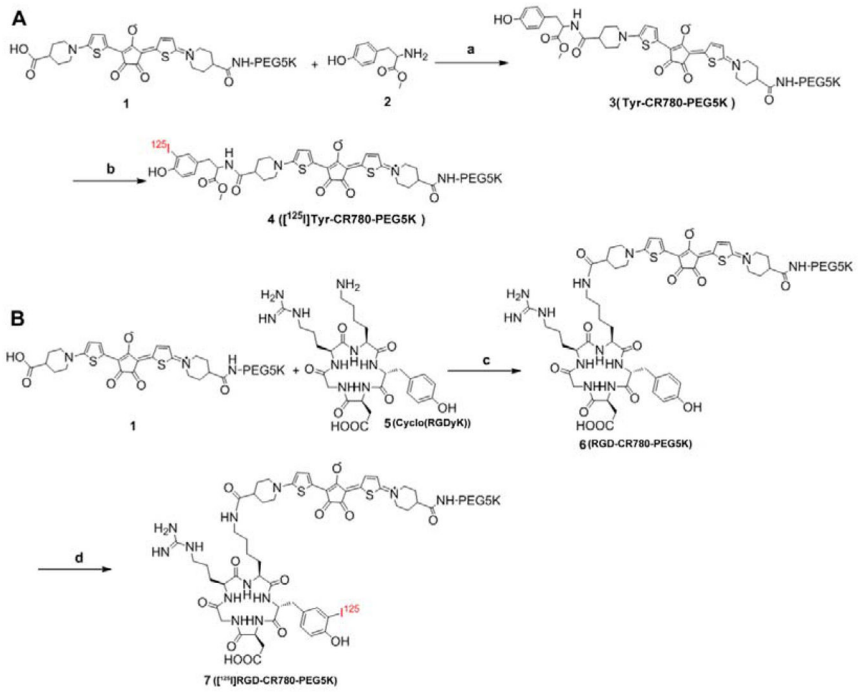

Scheme 1.

Synthesis of [^{125}I]Tyr-CR780-PEG5K (A) and [^{125}I]RGD-CR780-PEG5K (B). Reagents: (a), (c) EDC, NHS, DIPEA, CH_2Cl_2, 0 °C-r.t., 4 h, 85%; (b), (d) 1) [^{125}I]-NaI, Iodo-Gen, r.t., 3.5 min, 2) $Na_2S_2O_5$